Nitrate respiration and diel migration patterns of diatoms are linked in sediments underneath a microbial mat

Elisa Merz [1]*, Gregory J. Dick,[2] Dirk de Beer,[1]
Sharon Grim,[2] Thomas Hübener,[3] Sten Littmann,[1]
Kirk Olsen,[2] Dack Stuart,[4] Gaute Lavik,[1]
Hannah K. Marchant [1] and Judith M. Klatt [1,2]*

[1]Max Planck Institute for Marine Microbiology,
Celsiusstr. 1, Bremen, Germany.
[2]Geomicrobiology Lab, Department of Earth &
Environmental Sciences, University of Michigan, Ann
Arbor, Michigan.
[3]Department of Botany and Botanical Garden, University
of Rostock, Institute of Biosciences, Germany.
[4]University of Michigan, Cooperative Institute for Great
Lakes Research, Ann Arbor, Michigan.

Summary

Diatoms are among the few eukaryotes known to store nitrate (NO_3^-) and to use it as an electron acceptor for respiration in the absence of light and O_2. Using microscopy and ^{15}N stable isotope incubations, we studied the relationship between dissimilatory nitrate/nitrite reduction to ammonium (DNRA) and diel vertical migration of diatoms in phototrophic microbial mats and the underlying sediment of a sinkhole in Lake Huron (USA). We found that the diatoms rapidly accumulated NO_3^- at the mat-water interface in the afternoon and 40% of the population migrated deep into the sediment, where they were exposed to dark and anoxic conditions for ~75% of the day. The vertical distribution of DNRA rates and diatom abundance maxima coincided, suggesting that DNRA was the main energy generating metabolism of the diatom population. We conclude that the illuminated redox-dynamic ecosystem selects for migratory diatoms that can store nitrate for respiration in the absence of light. A major implication of this study is that the dominance of DNRA over denitrification is not explained by kinetics or

thermodynamics. Rather, the dynamic conditions select for migratory diatoms that perform DNRA and can outcompete sessile denitrifiers.

Introduction

In illuminated benthic ecosystems, microphytobenthos (MPB), a general grouping of benthic microalgae, drives primary production via photosynthesis. Due to their high productivity (Kühl *et al*., 1994), yet inconspicuous appearance, MPB-dominated ecosystems have been coined the 'secret garden' (Cahoon, 1999). Thriving at the thin interface of the water column and the sediment, many ecological aspects of this 'secret garden' derive from the dynamics of the local light climate and mass transport of metabolic substrates and products over a wide range of spatial and temporal scales (Boudreau and Jorgensen, 2001). To understand the controls on benthic primary production and nutrient cycling, it is crucial to link metabolic versatility and microbial behaviour, such as migration, to the spatio-temporal dynamics of physico-chemical parameters.

Diatoms are eukaryotic microalgae that often dominate MPB communities (Macintyre *et al*., 1996; Cahoon, 1999; Guarini *et al*., 2008; Longphuirt *et al*., 2009), where they exhibit metabolic flexibility and complex behavioural responses to environmental stimuli. It is well established that due to the interaction between migration of benthic diatoms and changes in the light climate and hydrodynamics, productivity varies with the tidal and diel light cycle (Serôdio and Catarino, 2000; Cartaxana *et al*., 2016). The ecological drivers for migration are multifaceted, ranging from the escape from grazing (Round and Palmer, 1966; Pinckney and Zingmark, 1991; Cartaxana *et al*., 2008) to light harvesting optimisation (Cartaxana *et al*., 2016), and are largely shaped by habitat-specific dynamics. Conversely, the migration behaviour of diatoms interacts with a variety of parameters crucial for the activity of other microbial inhabitants of the benthic realm. For instance, the migration rhythm is linked to the assimilation and respiration of inorganic nitrogen (Koho *et al*., 2011), which can have large effects

on the nitrogen (N)-cycle, particularly the balance between denitrification, dissimilatory nitrate/nitrite reduction to ammonium (DNRA) and nitrification (Daims *et al*., 2015). Intriguingly, diatoms themselves are capable of nitrate (NO_3^-) respiration via DNRA based on intracellularly stored NO_3^- – a rare capability among eukaryotic algae (Kamp *et al*., 2011; 2013; 2015). So far, the link between the metabolism of diatoms under dark anoxic conditions and their migration is poorly understood. Instead, the temporal metabolic switch to an anaerobic lifestyle has mainly been studied as a strategy for survival upon burial (Kamp *et al*., 2011).

To assess the impact of diatoms on the benthic N-cycle, it is crucial to consider their migration behaviour. The typical habitats for benthic diatoms are in coastal and neritic ecosystems, such as intertidal and subtidal mud and sand flats, estuaries, lagoons and sea-grass beds (Macintyre *et al*., 1996; Cahoon, 1999). Diatoms are also found in lakes, salt flats and thermal springs (Eldridge and Greene, 1994). In several of these environments, MPB communities form laminated microbial assemblages – microbial mats. These ecosystems portray highly dynamic microenvironmental conditions, which are primarily shaped by the interaction between local process rates and diffusional mass transfer. As their study is not complicated by advective mass transport dynamics mats represent an ideal natural laboratory to investigate the metabolic performance of diatoms during diel cycles.

Diatom-inhabited photosynthetic mats thrive under a low-O_2 water column in the Middle Island Sinkhole in Lake Huron, Michigan, USA (Ruberg *et al*., 2005). High-salinity, anoxic, cold and sulphate-rich groundwater emerges from an underwater source at ~24 m depth and cascades into the sinkhole area, creating a chemocline at the base of the Lake Huron water column. Due to the rare co-occurrence of illumination and low-O_2 bottom water, a unique benthic ecosystem flourishes. Thin cyanobacterial mats cover an area of ~10,000 m^2 of sediment, enriched in organic carbon originating from Lake Huron's pelagic productivity (Voorhies *et al*., 2012; Nold *et al*., 2013). Despite the extremely thin photic zone (<1 mm), the mat is functionally structured according to the light and redox gradients, comparable to other microbial mats (Stal *et al*., 1985; Gemerden, 1993; Stal and Caumette, 2013). The biogeochemical element cycling is shaped by the interaction of three main functional groups: motile oxygenic phototrophs, namely filamentous cyanobacteria and pennate diatoms, filamentous sulphide oxidizing bacteria, and sulphate reducing bacteria (Biddanda *et al*., 2006; 2015; Voorhies *et al*., 2012).

In situ observations (personal communication with divers, NOAA Thunder Bay National Marine Sanctuary) suggest that the diel dynamics of photosynthesis in the Middle Island Sinkhole mats can differ substantially from other mats. In some areas of the sinkhole, the mat apperance changes, as expected, from white at night to purple in the night to purple in the morning (Biddanda and Weinke, 2020), while in other areas, this migraton-driven structural shift is delayed to the afternoon. A similar migration lag has been observed in the Frasassi sulphidic springs, where, the cyanobacteria exclusively perform anoxygenic photosynthesis in the morning, and only transition to predominantly oxygenic photosynthesis in the afternoon (Klatt *et al*., 2020). This delay arises from competition of large sulphur oxidizing bacteria and cyanobacteria for the uppermost position in the mat and results in anoxic conditions in the photic zone for the majority of the illuminated fraction of the day (Klatt *et al*., 2016). Given that the diatoms are obligate oxygenic phototrophs but do not produce oxygen in this extended exposure time to anoxia, the question arises, how do they compete with the other phototrophs in such environments? We hypothesized that DNRA is the main respiratory pathway of diatoms in the Middle Island Sinkhole mats and that it accounts for a substantial fraction of diel metabolic activity. We used stable isotope incubations and light microscopy to determine how DNRA is linked to diel light dynamics and diatom migration behaviour. As N-loss from ecosystems and therefore eutrophication are largely determined by the balance between denitrification and DNRA (Kuypers *et al*., 2018), we determined contributions of both NO_3^- respiratory pathways and discuss the importance of intracellular storage and migration by diatoms for the benthic N-cycle.

Results and discussion

Benthos structure and diel variability

The microbial mat sampled from the Middle Island Sinkhole was less than 1 mm thick, coloured purple, white and/or brown and covered a fine-grained dark brown sediment. The coherent mat was not firmly attached to the fluid, soft, and organic-rich sediment; it was fragile and could only be sampled with a pipette, spoon or by careful core slicing. Due to microbial migration the colour of the mat surface changed during the day: the mat was white at night and until the early afternoon before transitioning to a purple-brown appearance. The dark brown colour of the sediment did not change during the diel cycle.

DNRA is the main NO_3^- reduction pathway in the benthos

The main pathway of NO_3^- reduction in the microbial mat and underlying sediment was determined using a $^{15}NO_3^-$ tracer approach in anoxic batch incubations in gastight glass vials containing sediment, mat or mat + sediment.

Most of the $^{15}NO_3^-$ could be recovered in the ^{15}N-ammonium ($^{15}NH_4^+$) pool and only a small amount was reduced to N_2, indicating that DNRA was responsible for 98%–99% of the NO_3^- consumption in all of the incubations (Fig. 1). These results show that DNRA, rather than denitrification, was the main NO_3^- reduction pathway in both the mat and sediment. However, dynamics of denitrification and DNRA differed. The production of N_2 by denitrification increased linearly throughout the 24 h time series in all of the incubations. In contrast, the NH_4^+ production rate by DNRA decreased after 2–5 h in the mat + sediment incubation (which had highest initial rates of DNRA (Table S1)). This decrease in DNRA occurred when a substantial proportion of the added $^{15}NO_3^-$ (30 μM) had been consumed. This suggests that the process of DNRA was limited by NO_3^- availability after 2–5 h while denitrification was not limited by NO_3^- throughout the incubation, even when concentrations became low. Therefore, the denitrifying community must
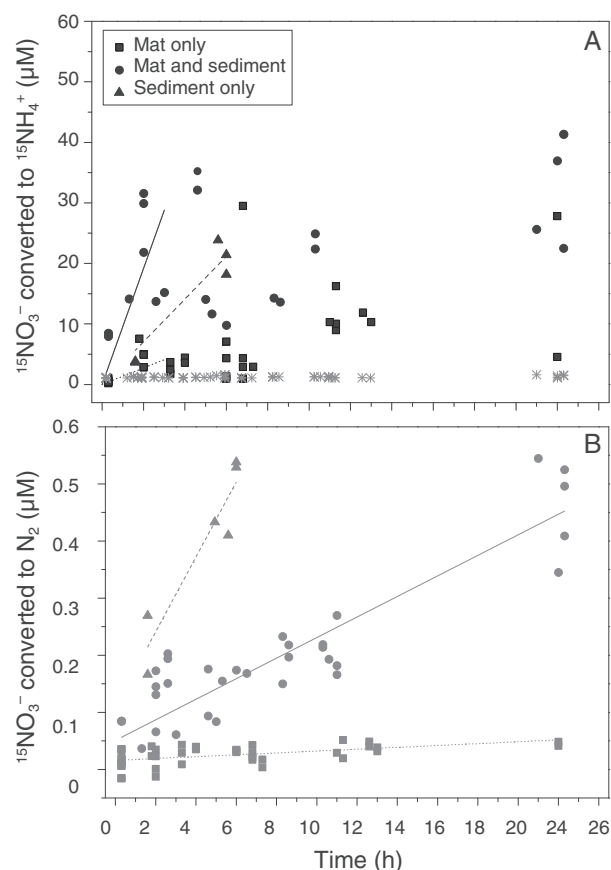
have a lower K_m value and thus a higher affinity for NO_3^- compared to the DNRA community, as also observed in other habitats (Behrendt et al., 2014). At the same time, the v_{max} was substantially lower, as evident from the constant rate of denitrification throughout the experiment, which suggests saturation with respect to NO_3^- concentration. Also, this rate was two orders of magnitude lower than the initial areal rates of DNRA before substrate limitation (Table S1). High affinity does therefore not seem to provide sufficient selective advantage in this ecosystem to yield a larger population size and/or cell specific activity than the DNRA performing community.

Interestingly, both denitrification and DNRA were lowest in the mat incubation without sediment – the only layer of the benthos that has diffusion-driven access to NO_3^- from the water column or possibly from nitrification under environmental conditions. Sediment with and without mat had the highest potential for NO_3^- respiration, which seems to contradict the absence of NO_3^- in the porewater under environmental conditions (Fig. 2A). This could indicate that the experimental conditions artificially stimulated DNRA and are not relevant in the ecosystem. If this were the case, we would have expected a lag period before DNRA commenced. Rather, the immediate and high rates of DNRA (particularly in comparison to the denitrification rates), suggest that microorganisms were
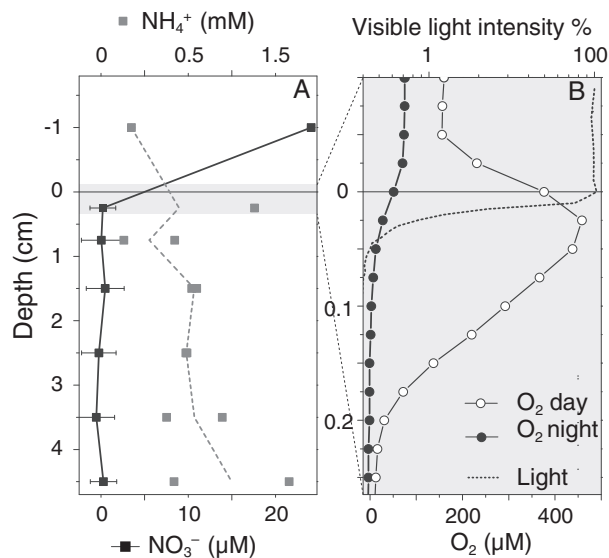

Fig 1. ^{15}N accumulated over time in the NH_4^+ (A) and N_2 (B) pools after addition of $^{15}NO_3^-$ to the water column overlying microbial mat on top of sediment, mat only and sediment slurry only. Note the difference in y-axis scale in (A) and (B). For illustration of the substantial differences in conversion rates we added data from panel (B) to panel (A) (grey asterisk). Lines were obtained by linear regression to estimate rates of denitrification and initial rates of DNRA (Table S1).

Fig 2. Depth profiles of NO_3^-, NH_4^+ and O_2 concentration, and light, in the mat and underlying sediment.
A. NO_3^- and NH_4^+ concentrations were measured in the porewater after extraction with Rhizons. The grey dashed line is the average NH_4^+ concentration in the two mat covered sediment cores.
B. Depth profile of scalar irradiance (400–700 nm) normalized to intensity at the mat surface was obtained from spectral microprofiling (note log scale). *In situ* O_2 profiles were measured with microsensors during the day (open symbols) and in the night (closed symbols).

already actively expressing the enzymes to carry out DNRA despite the apparent lack of NO_3^-. Therefore, NO_3^- is likely available in the sediment under environmental conditions. This is further supported by the observation that a combination of mat and sediment yielded highest rates of DNRA, even though the mat would be expected to hinder NO_3^- supply to the sediment from the water column. NO_3^- must thus be transferred to depth by other mechanisms than diffusion.

$^{15}NO_3^-$ is actively transported to deeper sediment layers

To investigate the depth distribution of DNRA under conditions that reflected those in the mats and sediments *in situ*, we added $^{15}NO_3^-$ to the water column overlying intact sub-cores with mat-covered sediment and followed $^{15}NH_4^+$ production over time and depth. DNRA occurred throughout day and night in the mat and sediment (Fig. 3A–D) and surprisingly, $^{15}NH_4^+$ production was detected to depths of 2–3 cm within 3 h after label addition. Diffusion of NO_3^- down to 3 cm would have taken 72 h, according to $\left(t = \frac{x^2}{2D}\right)$, where x is the mean diffusion distance of $^{15}NO_3^-$, during diffusion time t and where D is the NO_3^- diffusion coefficient ($1.73 \ 10^{-5} \ cm^2 \ s^{-1}$ at 21°C in water (Li and Gregory, 1974)). This means that the $^{15}NO_3^-$ must have been transported actively to deeper sediment layers.

Typical candidates for rapid NO_3^- storage and transport to the deep are large sulphur oxidisers, such as *Beggiatoaceae* (Schutte *et al*., 2018). However, the local *Beggiatoaceae* are freshwater non-vacuolated species (Sharrar *et al*., 2017) and therefore not likely to store NO_3^-. We finally excluded them as candidates for NO_3^- transport because intact *Beggiatoaceae* filaments were not observed in the deeper sediment by microscopy. The microscopic observations revealed the presence of motile diatoms, consistent with highly abundant chloroplast 16S rRNA genes in mat samples throughout the years (Fig. S2), and therefore we focussed on the diatoms. Chloroplast genes belonging to the Bacillariophyta were the most widely observed of identifiable 16S rRNA genes, contributing up to 46% of the reads in each mat sample. Although eukaryotic chloroplast 16S rRNA genes are not representative of eukaryotic abundance – due to the nonlinear relationships between chloroplast 16S rRNA gene copy number, organism, and growth (Green *et al*., 2011) – this observation suggests that diatoms are important members of the mat community.

Using light- and scanning electron microscopy we identified that *Craticula cuspidata* (Kützing) D.G. Mann, 1990 were the dominant epipelic diatoms in the microbial mat and sediment (Fig. S3). *C. cuspidata* thrives in brackish,
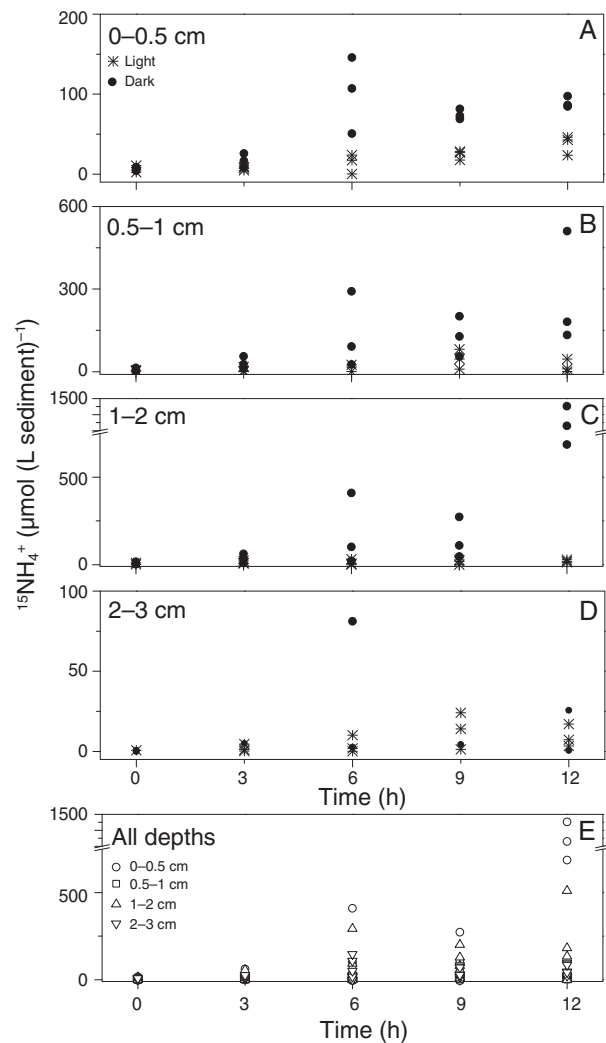

Fig 3. $^{15}NH_4^+$ concentration in porewater of sediment slices over time and depth (A–D). $^{15}NO_3^-$ was added to the water column above intact mat covered sediment cores in the morning (asterisks) and evening before darkening (black circles). In panels (A–D), symbols differentiate light and dark incubations while in panel (**E**) all depths from A–D are shown on the same scale with no differentiation of light versus dark.

as well as eutrophic, environments and can be differentiated very well within the *Craticula* genus due to their size (115–120 × 27–29 μm) and characteristic outline (Fig. S3). As the potential for NO_3^- storage of *C. cuspidata* has not been tested previously, we separated the cells from the sediment, measured intracellular NO_3^- concentration, and found that they stored NO_3^- at 83 ± 25 fmol cell^{-1}. Assuming a cylindrical diatom volume of 37.7 pl, the intracellular concentration would be ~2.2 mM and hence, concentrations within the vacuole must be even higher. We also confirmed that these diatoms instantaneously accumulate $^{15}NO_3^-$ by exchange with their internal reservoir (Fig. S4). This process differs from active NO_3^- uptake and can be explained by

transmembrane counterflow. Briefly, the immediate exchange of the stored ^{14}N to ^{15}N in the cells is due to the energetically neutral exchange in steady state (Xie, 2008). Thus, *C. cuspidata* are able to accumulate $^{15}NO_3^-$ instantaneously, given that they already have an internal NO_3^- pool. After this tracer uptake, the diatoms would have had to migrate at least down to 2–3 cm depth within 3 h to explain the production of $^{15}NH_4^+$, which is in line with a migration speed of up to 1.7 cm h^{-1} as observed in mudflat sediment (Hay *et al.*, 1993). Taken together, the data imply that diatoms with an internal NO_3^- reservoir resided at the surface during $^{15}NO_3^-$ addition and accumulated the tracer instantaneously by transmembrane counterflow before transporting it into anoxic sediment layers, whereupon it was respired to NH_4^+.

NO_3^- reduction rates and C. cuspidata *migrate over a diel cycle*

DNRA rates measured in the 'anoxic batch incubations' were highly variable (Fig. 1). To determine if NO_3^- was only supplied to the mat and sediment by diffusion or actively transported into the sediment, the distribution of rates over depth within the sediment was determined in intact, mat-covered sediment cores after addition of $^{15}NO_3^-$ to the water column. These incubations on showed that rates in deeper sediment layers were higher when $^{15}NO_3^-$ was added in the evening (18:00 h) (Fig. 3). These results suggest a link between the abundance of *C. cuspidata* at the surface and the occurrence of DNRA, likely because light and/or a circadian migration rhythm shape the NO_3^- uptake at the mat-water-interphase.

To uncouple DNRA rate measurements from the timing of NO_3^- uptake, we injected $^{15}NO_3^-$ through intact subcores over a 24 h period and measured the NH_4^+ production rates over depth. While DNRA always occurred, its magnitude varied depending on time of day (Fig. 4A, Table S2). A clear rate maximum moved vertically through the sediment over a diel cycle. In the late afternoon, this NH_4^+ production peak detached from the surface and reached its maximum depth of ~3–4 cm at ~0:00 h. In the early morning, the rate maximum shifted upwards again, reaching 0.5–1 cm before noon (Fig. 4A). In the late afternoon, NH_4^+ production rates were minimal in both the sediment and the mat at all depths. This DNRA minimum coincided with a colour change from white to brown at the surface of the mat. Overall, DNRA rates in the sediment were closely related to the migration pattern of the diatoms (compare Fig. 4A and Fig. 4B). We cannot exclude that a bacterial DNRA-performing community in the deep sediment is fuelled by NO_3^- released from *C. cuspidata* on their journey.

However, it is well established for other genera of diatoms that they are capable of DNRA (Kamp *et al.*, 2011; 2013). Further, we consider it unlikely that *C. cuspidata* do not respire during migration through anoxic sediment, and there is no evidence that diatoms use electron acceptors other than O_2 and NO_3^-. Thus, the correlation between DNRA maxima and viable diatom abundance strongly suggests that DNRA is predominantly performed by *C. cuspidata*.

Only ~40% of the diatom population migrated deeply into the sediment and tracked the DNRA rate maximum (Fig. 4B, Table S3). The remaining 60% of the population stayed within the uppermost 5 mm, although not directly at the surface. DNRA rates in this uppermost section were highest immediately after the onset of darkness, then decreased and remained highly variable. As anoxic conditions persist in the lower boundary of this layer even in the presence of oxygenic photosynthesis (Fig. 2C), the near-surface residing diatom subpopulation might contribute to the occasionally high DNRA rates. We cannot exclude that a sessile DNRA performing community was driving these rates in the uppermost section. Nevertheless, the correlation of the deep migration and DNRA pattern, together with the observation that a large subpopulation resides at the surface, indicates that DNRA both in the sediment and mat can be explained by diatom activity.

Migration is the key to success

Motile benthic diatoms often undergo vertical migration according to diurnal and tidal cycles in intertidal sediments to escape grazing or hydrodynamic stress (Round and Palmer, 1966; Pinckney and Zingmark, 1991; Cartaxana *et al.*, 2008). Migration patterns are thus usually regulated by the tidal rhythm and even remain active for 3–11 days (Palmer and Round, 1967) after transfer of diatoms to a stagnant environment. In Lake Huron, changes in water level are not dependent on tides, and internal waves do not occur with a fixed rhythm that could explain the *C. cuspidata* migration pattern. Changes in the light regime, and thus the diel light cycle, can also trigger downward migration of diatoms, yet light in the Middle Island Sinkhole mats only penetrates down to ~750 μm (Fig. 2B). *C. cuspidata* might thus use phototaxis during migration initiation and for micro-cycling in the uppermost 5 mm but it cannot explain behaviour in the deep. Similarly, encountering anoxia is has been shown to stop downwards migration and initiate return of some diatom species to the surface (Kingston, 1999), while *C. cuspidata* migrate through sulfidic and anoxic sediment. Phosphate and silicate gradients can also guide deep migration (Karen *et al.*, 2019) and gravitaxis (Frankenbach *et al.*, 2014) might also aid this navigation.
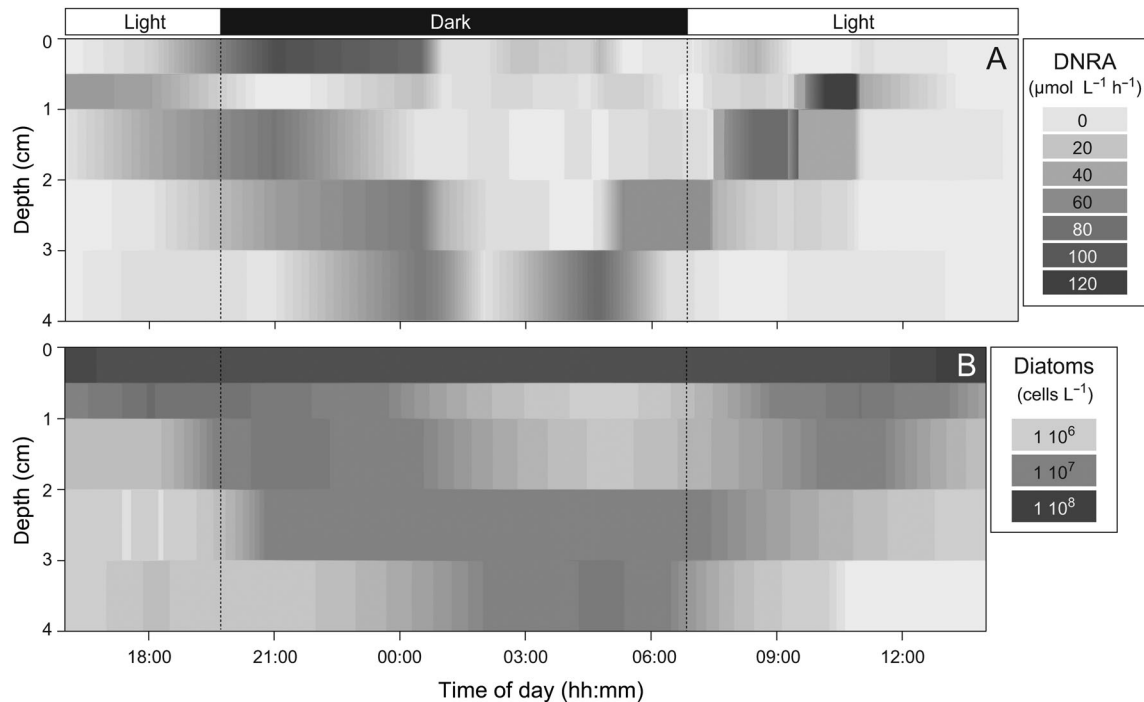
Fig 4. Depth profiles of NH_4^+ production rates (A) and diatom abundance (B) over the course of day. Bars on top of (A) indicate light conditions. L^{-1} = (L sediment)$^{-1}$. Diatom cell density is plotted on a log scale.

However, these do not appear to be the stimuli that trigger descent and ascent of the DNRA-performing *C. cuspidata* in the Middle Island Sinkhole.

The most straightforward explanation for the unusual migration behaviour of *C. cuspidata* would be a regulation mechanism based on NO_3^- storage capacity. For marine *Beggiatoaceae*, the electric potential over the vacuolar membrane changes with the internal NO_3^- concentration (Mussmann *et al.*, 2007; Beutler *et al.*, 2012). It seems likely that such potential change also occurs in diatoms during depletion of NO_3^-, 'signalling' *C. cuspidata* to resurface to replenish NO_3^- from the water column and thus triggering upward migration. As a single *C. cuspidata* cell stores 83 ± 25 fmol NO_3^- intracellularly, this internally stored NO_3^- would last for 12.6 h, calculated based on an average production rate of 6.6 fmol NH_4^+ cell^{-1} h^{-1} (Tables S1 and S2). This capacity is strikingly close to the duration of one migration cycle ($\sim$18–20 h), suggesting that the amount of NO_3^- in the vacuole could indeed play a regulatory role in migration behaviour and separation of diatom populations. Furthermore, DNRA rates associated with the subpopulation that stays near the surface (Figs 4 and 5) decreased after only a few hours of darkness, suggesting that NO_3^- became limiting. In contrast, the deep migrating population continuously performs DNRA. This indicates that deep migration is only initiated when intracellular NO_3^- concentrations are sufficiently high to

guarantee energy supply during the 18 h of deep migration. While separation into subpopulations has previously been linked to reproduction cycles, with cells migrating to depth for cell division (Saburova and Polikarpov, 2003), vacuolar NO_3^- content thus offers an alternative explanation for initialisation of deep migration and separation of populations.

While the physical and chemical stimuli guiding *C. cuspidata* through the dark sediments are at the moment unresolved, it is clear that migration and energy investment into NO_3^- storage for anaerobic respiration is advantageous to the diatoms. *C. cuspidata* does not reside at the mat surface for most of the day; it performs anaerobic respiration in the deep anoxic sediment instead. This appears paradoxical, as these typical oxygenic phototrophs harvest light for only $\sim$5 h. Even the near-surface residing subpopulation remaining in the uppermost 5 mm – but not at the mat surface – does not have access to light for most of the day as light penetrates only down to <1 mm. This behaviour contradicts any energetic consideration and can only be explained in the context of interaction with other microorganisms and the environment. Thus, migration coupled to DNRA and the resultant circumvention of an interaction with cyanobacteria, must represent an important competitive advantage. The long absence from the surface implies that diatoms are only directly competing with the cyanobacteria during their short phase of oxygenic photosynthesis. Competition is
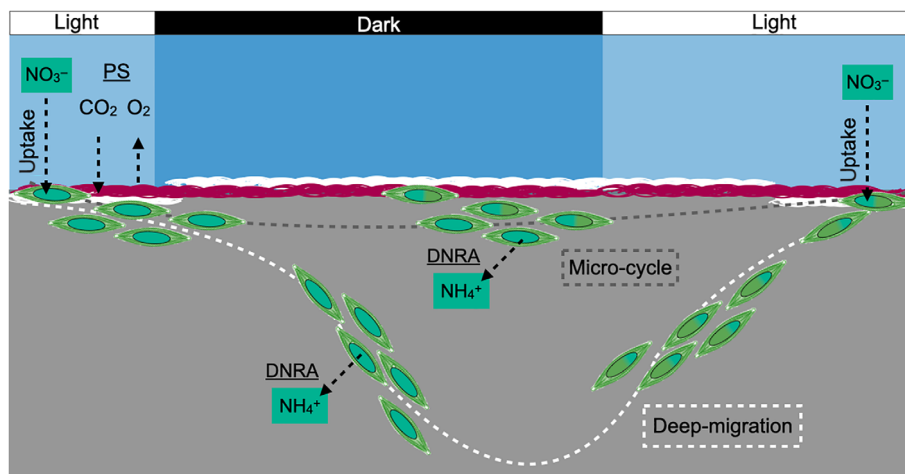
Fig 5. A diel cycle in the Middle Island Sinkhole (modified after (Consalvey *et al.*, 2004). *Craticula cuspidata* perform photosynthesises (PS) in the afternoon and accumulate NO_3^- (turquoise ellipses = stored NO_3^-) from the water column. In the early evening deep vertical migration of a subpopulation is initiated (deep migration = white dotted line), and the intracellular NO_3^- reservoir is respired via DNRA. This subpopulation only returns to the surface in the early afternoon of the next day, which coincides with a change of mat structure: The white *Beggiatoaceae*-dominated surface layer disappears, and purple cyanobacteria and diatoms are visible. DNRA rates are negligible at this time of day because the diatoms are at the mat surface performing oxygenic photosynthesis. The other *C. cuspidata* subpopulation resides within the first 5 mm of the mat and sediment for the complete diel cycle and shows a micro-cycling behaviour (Micro-cycling = grey dashed line) performing oxygenic photosynthesis or DNRA, depending on the time of day and position in the mat.

likely based on light access, as the spectral range of light reaching the mat surface is very narrow (400–600 nm, Fig. S1). Both phototrophs possess chlorophyll a which has absorption maxima at 465 nm and 665 nm (Stomp *et al.*, 2007). The local cyanobacteria are additionally equipped with phycocyanin, phycoerythrin and phycoerythrocyanin (Voorhies *et al.*, 2012) to absorb light at between 500–600 nm, whereas diatoms possess fucoxanthin, also providing absorbance in this spectral range (Stomp *et al.*, 2007; Kuczynska *et al.*, 2015). Thus, the spectral niche of diatoms and cyanobacteria overlap. Their ecological niches are, however, separated for the rest – the majority – of the day. The cyanobacteria perform anoxygenic photosynthesis in the morning (Klatt *et al.*, 2020) and might perform fermentation, aerobic or anaerobic S^0-based respiration at night (Stal and Moezelaar, 1997). Diatoms meanwhile switch to DNRA, which implies niche separation and thus facilitation of coexistence (Gause *et al.*, 1936).

In addition to internal competition within the mats, avoidance of predation, e.g. by occasionally observed gastropods, might be an important factor selecting for migration (Consalvey *et al.*, 2004). Furthermore, the flow velocity of ground water can vary substantially over days to seasons, which can lead to irregularly occurring mat disruption events, leaving uncovered sediment behind (pers. comm. with divers who sampled, NOAA Thunder Bay National Marine Sanctuary). Diatoms hidden in the deep sediment would likely be the first colonizers after such events. This is consistent with observations after

mat subsampling in the lab: *C. cuspidata* were the first organism to repopulate the sediment surface (within minutes to hours), while the filamentous cyanobacteria had to migrate horizontally from the peripheral, intact mat. Hence, the ability to migrate overall enhances the chance of survival during disturbance events such as grazing or mat disruption, and allows rapid recolonisation.

Implications for the nitrogen cycle

The controlling factors that determine whether DNRA or denitrification is dominant in a habitat are a subject of debate. In the past studies have focussed on the impact of kinetics (King and Nedwell, 1985; Tiedje, 1988; Behrendt *et al.*, 2014; Kraft *et al.*, 2014; McTigue *et al.*, 2016; Murphy *et al.*, 2020), inhibition and/or thermodynamics (Dong *et al.*, 2011; Kraft *et al.*, 2014; Bonaglia *et al.*, 2017; Dolfing and Hubert, 2017). The dominance of DNRA in the benthos may be explained by selection for a particular NO_3^- reducing community based on other adaptation strategies beyond the NO_3^- reduction pathway. Hence, in this habitat the balance between DNRA and denitrification is not determined by inhibition- or substrate kinetics, or by thermodynamics, but by composition of the NO_3^--reducing community, which is dominated by a diatom species that efficiently accumulates NO_3^- and migrates for almost an entire diel cycle, meanwhile performing DNRA and not denitrification. In other ecosystems migration coupled to NO_3^-

respiration may be favourable for other microorganisms, potentially equipped with the denitrification pathway instead, as observed in non-illuminated sediments, such as off the coast of California (Prokopenko *et al.*, 2011) or in the deep sea (Schutte *et al.*, 2018).

In the Middle Island Sinkhole, DNRA is daily routine for diatoms and is intimately linked to their migration to deeper sediments. *C. cuspidata* usually inhabit fine-grained freshwater sediments with elevated electrolyte content but are cosmopolitan and might therefore show similar behaviour in many other ecosystems. The potential for NO_3^- storage and respiration via DNRA, and migration, is not limited to specific illuminated freshwater systems but is spread across phyla and ecosystems (Stief *et al.*, 2014; Kamp *et al.*, 2015; Schutte *et al.*, 2018). For instance, in intertidal sediment conditions similar to the Middle Island Sinkhole – illumination and regular anoxia – are met and 'secret gardens' (Cahoon, 1999) flourish. Also, eukaryotic NO_3^- storage has been confirmed and migratory organisms are abundant (Cartaxana and Serôdio, 2008). This raises the question if DNRA in redox-dynamic ecosystems has been underestimated, as most studies on DNRA do not state specifically that they took diel or tidal rhythms into account. For instance, patchy DNRA rates at the same sampling site could be explained by the lack of diatoms in the sample, destruction of gradients guiding migration or by sampling during times when the diatoms have not accumulated NO_3^- (Sundbäck *et al.*, 2000; Risgaard-Petersen, 2003; Giblin *et al.*, 2013; Decleyre *et al.*, 2015). The role of DNRA in the biogeochemical N-cycle can therefore only be assessed by considering the importance of migrating organism and the corresponding adjustment of sampling timing.

C. cuspidata is a key player in the 'secret garden' (Cahoon, 1999) studied here because it can flexibly transition between energy sources, namely between using light during a short fraction of the day and chemical energy for most of their daily life (Fig. 5). This flexibility coupled their ability to store the electron-acceptor NO_3^- enables *C. cuspidata* to migrate into anoxic sediments, removing it from direct competition to other microorganisms and allowing it to escape predation and hydrodynamic stress. This ecological strategy makes the diatoms one of the most abundant taxa in the Middle Island Sinkhole mat as well as underlying sediment, and fundamentally shapes the benthic N-cycle by retaining N in the system.

Experimental procedures

Sampling

Sediment cores (25 cm diameter, 20–25 cm sediment sampling depth) were taken by SCUBA divers at approximately 24 m depth in the Middle Island Sinkhole (45°11.941 N, 83°19.671 W). Sampling took place in 2012–2017 for 16S sequencing; and in May 2017, June 2018, and July 2019 for activity measurements. Mat sampling sites were chosen based on brownish appearance of the mat surface, indicative of diatom presence. Bottom water was retrieved using 30 m of oxygen impermeable tubing (Masterflex, Merck) and a peristaltic pump (Masterflex) placed on deck. Sediment cores and water samples were transported cooled and in the dark to the laboratory in Ann Arbor, Michigan. In the laboratory, the cores were kept at *in situ* temperature (12°C) in a thermostated water bath. The mats were illuminated at 90 μmol photons m^{-2} s^{-1} by LED light sources, which is in the higher range of values measured *in situ* in proximity of the mat surface (Fig. S1a). To mimic environmental light quality, optical filter foil (cut-off $\lambda \approx 600$ nm; Fig. S1b and c) was used. Cores were kept on a 12 h:12 h light:dark cycle to approximate the natural light cycle.

16S sequencing and analysis

Samples for 16S sequencing were collected by carefully removing the mat layer from freshly retrieved cores and immediate flash-freezing on-board. DNA extractions were performed using the MPBio Fast DNA Spin Kit for Soil (MP Biomedical, USA) with modifications (see Supplementary Information). DNA samples were submitted to the University of Michigan Host Microbiome Core for Illumina library preparation and sequencing (Seekatz *et al.*, 2015; Kozich *et al.*, 2013) (see Supplementary Information).

Minimum Entropy Decomposition v. 2.1 (Eren *et al.*, 2015) was used to analyse merged and quality trimmed sequencing reads (see Supplementary Information). GAST (Huse *et al.*, 2008) and BLASTN were used to call taxonomy using the curated SILVA database (Pruesse *et al.*, 2007) and PhytoRef (Decelle *et al.*, 2015). Chimera checks were performed using mothur v. 1.33 (Schloss *et al.*, 2009). The R statistical environment (R Core Team, 2015) in RStudio (RStudio Team 2014) was used to analyse nodes.

O₂ microprofiles

O₂ microsensors for *in situ* profiling were built and calibrated as described by (Revsbech, 1989). Depth profiles were acquired in July 2016 using a microprofiler as previously described (Wenzhöfer *et al.*, 2000; De Beer *et al.*, 2006).

In situ *hyperspectral light profiles*

Seven *in situ* spectral profiles were collected in the sinkhole and in open water in 2015–2016. Profiles were

collected using a Sea-Bird HyperPro II profiler equipped with up- and down-facing HyperOCR radiometers measuring wavelengths 348–801 nm (bin size = 3.3 nm), plus an identical fixed surface radiometer to record sky conditions (Bosse *et al.*, 2019). The profiler was deployed on the sunny side of the vessel and allowed to free-fall through the water column to avoid the vessel shadow. A duplicate cast was collected as soon as the profiler was returned to the surface to capture identical light conditions. Data were processed using ProSoft (Sea-Bird) proprietary software.

Ex-situ *light micro-profiles*

Light penetration depth was determined *ex-situ* in a mat-covered sediment core using a scalar irradiance probe with a 100 μm tip (Zenzor, Denmark) on a motorized vertical positioner, after (Kühl and Jørgensen, 1992). The light sensor was connected to a USB400-FL Spectrometer (Ocean Optics, USA). A halogen light source (Schott, KL 1500) was used for illumination of the mat during measurements.

Porewater

Porewater was collected from freshly collected sediment cores on-board in 0.5–1 cm-intervals down to 5 cm using 2 cm long Rhizons (Rhizosphere Research Products, Netherlands) in July 2019. Per depth, only ∼500 μl were extracted including volume of the Rhizon and tubing to minimize smearing effects between depths. Porewater was flash frozen on board, immediately after sample collection. NO_x concentration ($\sum NO_2^-$, NO_3^-) was subsequently determined using a chemiluminescence detector after reduction to NO with 90°C acidic Vanadium(III)chloride (Braman and Hendrix, 1989). NH_4^+ in the porewater samples was determined colorimetrically according to (Holmes *et al.*, 1999).

Stable isotope incubations

To determine the contribution of denitrification and DNRA to NO_3^- reduction rates, a $Na^{15}NO_3^-$ (99% CP, CAS:31432–45-8, Sigma-Aldrich) tracer method was used. Batch incubations were performed of (i) a mixture of mat and sediment, (ii) sediment and (iii) only microbial mat on agarose. First, sediment was homogenized and 6 ml were transferred into 12 ml gas-tight glass vials with a septum cap (Exetainer, Labco). The vials were filled with He-degassed, filtered bottom water (0.45 μm PES membrane) without headspace. After settling of sediment, we placed pieces of mat on the sediment surface, and briefly purged the water column with He again to ensure that oxygen in the vials was exclusively

introduced by photosynthetic production. A subset of the vials was left with bare sediment. An additional set of exetainers was filled with 6 ml agarose (1.5%) instead of sediment. Filtered bottom water was added and purged with He for 30 min every few hours over several days until the agarose was anoxic down to at least 2.5 cm, as confirmed with O_2 microsensor measurements. Subsequently, mat pieces were placed on the agarose, following the same procedure as for the sediment incubations. The agarose was used to ensure comparable water column volume and distance to the light source among the different treatments. The vials were exposed for 1–2 h to darkness to deplete remaining NO_3^- as well as residual O_2 in the water column. The absence of oxygen was confirmed in three of the exetainers dedicated to microsensor measurements. $^{15}NO_3^-$ was injected into the water column from a He-purged stock solution using gas-tight glass syringes (Hamilton, Australia). To achieve approximately homogenous distribution of the label in the water column, injections were done by holding the plunger in the fixed position and slowly pulling up the syringe, starting at the mat or sediment surface. Incubations were stopped in 1.5–4 h intervals over ∼24 h by injecting 50 μl saturated $HgCl_2$. To prevent precipitation of Hg^{2+} with sedimentary sulphide, we simultaneously added 200 μl 10% $ZnCl_2$ through the septum. Injections were followed by rigorous mixing. The isotopic composition of N_2 and NH_4^+ at each time point was determined after replacing 2 ml of the water in the incubation vial with a helium headspace and transferring the subsampled 2 ml into a 6 ml glass vials prefilled with 2 ml 0.35% NaCl solution. Gas from the headspace of the incubation vial was injected directly into a GC-IRMS (isoprime precisION, elementar, UK) and the isotope ratios of $^{28}N_2$:$^{29}N_2$ and $^{28}N_2$:$^{30}N_2$ were determined (Holtappels *et al.*, 2011). The concentration of $^{29}N_2$ and $^{30}N_2$ were subsequently calculated from the excess of each relative to an air sample. $^{15}NH_4^+$ concentrations were determined in the same way from the subsampled liquid after rigorous purging with He and oxidation of NH_4^+ with hypobromite to N_2. $^{15}NH_4^+$ and $^{15}N_2$ production rates were calculated based on the increase of $^{15}NH_4^+$ and $^{29}N_2$ + $^{30}N_2$ concentration over time, and subsequently converted into areal rates across the sediment/mat surface based on the area exposed to the tracer (Warembourg, 1993; Preisler *et al.*, 2007; Marchant *et al.*, 2016).

To distinguish between NO_3^- diffusion or active transport into deeper sediment, the DNRA rates over depth within the sediment was determined in intact, mat-covered sediment cores after addition of $^{15}NO_3^-$ to the water column. First, 3 large sampler cores (25 cm diameter) were subsampled using smaller cores (7 mm diameter) that were pushed ∼6 cm deep into the sediment. These sub-cores were darkened with black tape up to

the mat surface to ensure illumination only from above. Using a gas-tight syringe (Hamilton, Australia) $^{15}NO_3^-$ was added to the water column of each sub-core at either 6.00 h or 18.00 h, reaching a final concentration of 200 μM $^{15}NO_3^-$ in the bottom water. Subsets of the cores were sectioned in 1 cm depth intervals every 3 h. The slices were immediately submerged in 1 ml ultrapure water spiked with 50 μl saturated $HgCl_2$ and 200 μl 10% $ZnCl_2$ solutions to stop the incubation. $^{15}NH_4^+$ concentration in these slurries was determined by transferring the supernatant into septum vials and following the conversion procedure described above.

In a third stable isotope experiment, we assessed the temporal and spatial dynamics of DNRA rates dependent on time of day by injecting $^{15}NO_3^-$ into mat and sediment of the 7 mm sub-cores. To ensure a vertically homogenous distribution of the tracer, the injection was done by slowly pushing up a syringe filled with $^{15}NO_3^-$ stock solution while keeping the plunger in a fixed position. Core slicing, sample preparation and mass spectrometry were conducted as described above.

Depth profiles of diatom abundance determined by microscopy

The depth distribution of motile diatom cells over a light–dark cycle (12:12 h) was determined by sectioning sub-cores (see above) in regular time intervals, separation of viable diatom cells from sediment and cell counting. Specifically, sediment slices were transferred into a conical centrifuge tube filled with filtered *in situ* water. The tube was covered with black tape except for an uncovered area (∼3 mm^2) on the side of the tube, which was illuminated by a Schott lamp (∼300 μmol photons m^2 s^{-1}). We harvested the cells that had migrated towards the light and accumulated on the side of the tube, and suspended them in 1 ml filtered *in situ* water. Diatoms were counted using a light microscope and a counting chamber (Neubauer improved, Germany).

Scanning electron microscopy

Subsamples of the diatoms harvested based on their phototaxis (see above) were conserved by flash freezing for Scanning Electron Microscopy (SEM) imaging. Samples were prepared on small chips of Si- and GaAs-wafer material. To preserve the surface structure of all cells in the sample the material was dehydrated using critical point drying before SEM imaging, after water removal by an ethanol series with increasing ethanol concentrations (30%, 50%, 70%, 80% and 96%). The ethanol in the sample was removed by critical point drying (Leica EM CPD300 Wetzlar, Germany). Secondary electron (SE) micrograph images were taken using a Quanta 250 FEG (FEI, Eindhoven, The Netherlands) with an accelerating voltage of 2 and 10 kV.

NO$_3^-$ storage and tracer uptake by diatoms

To quantify intracellular NO_3^- storage capacity, diatoms were harvested from the top of the mat by gentle elution with water from a Pasteur pipette and collection of water column with the suspended cells. We then enriched the viable cells as described above based on their phototaxis and suspended them in filtered *in situ* water. NO_3^- concentration in the *in situ* water with and without diatoms was measured using a chemiluminescence detector as described in the 'porewater' section. Assuming that the diatoms lysed, releasing all intracellular NO_3^- when injected into the 90°C acidic Vanadium(III)chloride solution, we calculated the concentration of stored NO_3^- based on the difference to the cell-free control. A subsample of the injected diatom suspension was used for cell counting. Internally stored NO_3^- per diatom and intracellular concentration were estimated by assuming a cylindrical diatom shape.

To determine the rate of exchange of stored unlabelled NO_3^- with externally supplied $^{15}NO_3^-$, diatoms pre-fed for 24 h with $^{14}NO_3^-$, were transferred to $^{15}NO_3^-$-amended *in situ* water. Specifically, after a washing step in filtered *in situ* water without NO_3^-, aliquots of 1 ml cell suspension were added to 10 ml of filtered, He-degassed bottom water amended with 20 μM $^{15}NO_3^-$ and incubated in the dark. The incubation was stopped after 0, 10, 20 and 30 min by filtering the tube contents. The filter was washed with 10 ml deionized water and immediately frozen in liquid N$_2$. To release internally stored NO_3^-, the filters were submerged in ultrapure water and exposed to thaw–freeze cycles (Stief *et al.*, 2013). $^{15}NO_3^-$ concentration in these cracked diatom samples was measured after $^{15}NO_2^-$ removal using sulfamic acid. Spongy cadmium was applied to reduce $^{15}NO_3^-$ to $^{15}NO_2^-$. To reduce $^{15}NO_2^-$ to N$_2$ an additional sulfamic acid treatment was conducted (Füssel *et al.*, 2012). The isotope ratio in the resultant N$_2$ pool was measured from the headspace using GC-IRMS as described above (Marchant *et al.*, 2016).

Conflict of interest

All authors declare no conflict of interest.

References

Behrendt, A., Tarre, S., Beliavski, M., Green, M., Klatt, J., de Beer, D., and Stief, P. (2014) Effect of high electron donor supply on dissimilatory nitrate reduction pathways in a bioreactor for nitrate removal. *Bioresour Technol* **171**: 291–297. https://doi.org/10.1016/j.biortech.2014.08.073.

Beutler, M., Milucka, J., Hinck, S., Schreiber, F., Brock, J., Mussmann, M., *et al*. (2012) Vacuolar respiration of nitrate coupled to energy conservation in filamentous Beggiatoaceae. *Environ Microbiol* **14**: 2911–2919. https://doi.org/10.1111/j.1462-2920.2012.02851.x.

Biddanda, B.A., Coleman, D.F., Johengen, T.H., Ruberg, S. A., Meadows, G.A., Van Sumeren, H.W., *et al*. (2006) Exploration of a submerged sinkhole ecosystem in Lake Huron. *Ecosystems* **9**: 828–842. https://doi.org/10.1007/s10021-005-0057-y.

Biddanda, B.A., McMillan, A.C., Long, S.A., Snider, M.J., and Weinke, A.D. (2015) Seeking sunlight: rapid phototactic motility of filamentous mat-forming cyanobacteria optimize photosynthesis and enhance carbon burial in Lake Huron's submerged sinkholes. *Front Microbiol* **6**: 1–13. https://doi.org/10.3389/fmicb.2015.00930.

Biddanda, B.A., & Weinke, A.D. (2020) Extant mat world analog microbes synchronize migration to a diurnal tempo. *Earth and Space Science Open Archive*. https://doi.org/10.1002/essoar.10502762.1.

Bonaglia, S., Hylén, A., Rattray, J.E., Kononets, M.Y., Ekeroth, N., Roos, P., *et al*. (2017) The fate of fixed nitrogen in marine sediments with low organic loading: an *in situ* study. *Biogeosciences* **14**: 285–300. https://doi.org/10.5194/bg-14-285-2017.

Bosse, K.R., Sayers, M.J., Shuchman, R.A., Fahnenstiel, G. L., Ruberg, S.A., Fanslow, D.L., *et al*. (2019) Spatial-temporal variability of *in situ* cyanobacteria vertical structure in Western Lake Erie: implications for remote sensing observations. *J Great Lakes Res* **45**: 480–489. https://doi.org/10.1016/j.jglr.2019.02.003.

Boudreau, B.P., and Jorgensen, B.B. (eds). (2001) *The Benthic Boundary Layer: Transport Processes and Biogeochemistry*, Oxford, England: Oxford University Press.

Braman, R.S., and Hendrix, S.A. (1989) Nanogram nitrite and nitrate determination in environmental and biological materials by vanadium(III) reduction with chemiluminescence detection. *Anal Chem* **61**: 2715–2718. https://doi.org/10.1021/ac00199a007.

Cahoon, L. (1999) The role of benthic microalgae in neritic ecosystems. *Oceanogr Mar Biol* **37**: 47–86.

Cartaxana, P., and Serôdio, J. (2008) Inhibiting diatom motility: a new tool for the study of the photophysiology of intertidal microphytobenthic biofilms. *Limnol Oceanogr Methods* **6**: 466–476. https://doi.org/10.4319/lom.2008.6.466.

Cartaxana, P., Brotas, V., and Serôdio, J. (2008) Effects of two motility inhibitors on the photosynthetic activity of the diatoms cylindrotheca closterium and *Pleurosigma angulatum*. *Diat Res* **23**: 65–74. https://doi.org/10.1080/0269249X.2008.9705737.

Cartaxana, P., Cruz, S., Gameiro, C., and Kühl, M. (2016) Regulation of intertidal microphytobenthos photosynthesis over a diel emersion period is strongly affected by diatom migration patterns. *Front Microbiol* **7**: 1–11. https://doi.org/10.3389/fmicb.2016.00872.

Consalvey, M., Paterson, D.M., and Underwood, G.J.C. (2004) The ups and downs of life in a benthic biofilm: migration of benthic diatoms. *Diat Res* **19**: 181–202. https://doi.org/10.1080/0269249x.2004.9705870.

Daims, H., Lebedeva, E.V., Pjevac, P., Han, P., Herbold, C., Albertsen, M., *et al*. (2015) Complete nitrification by Nitrospira bacteria. *Nature* **528**: 504–509. https://doi.org/10.1038/nature16461.

De Beer, D., Sauter, E., Niemann, H., Kaul, N., Foucher, J. P., Witte, U., *et al*. (2006) *In situ* fluxes and zonation of microbial activity in surface sediments of the Håkon Mosby Mud Volcano. *Limnol Oceanogr* **51**: 1315–1331. https://doi.org/10.4319/lo.2006.51.3.1315.

Decelle, J., Romac, S., Stern, R.F., Bendif, E.M., Zingone, A., Audic, S., *et al*. (2015) PhytoREF: a reference database of the plastidial 16S rRNA gene of photosynthetic eukaryotes with curated taxonomy. *Mol Ecol Resour* **15**: 1435–1445. https://doi.org/10.1111/1755-0998.12401.

Decleyre, H., Heylen, K., Van Colen, C., and Willems, A. (2015) Dissimilatory nitrogen reduction in intertidal sediments of a temperate estuary: small scale heterogeneity and novel nitrate-to-ammonium reducers. *Front Microbiol* **6**: 1124. https://doi.org/10.3389/fmicb.2015.01124.

Dolfing, J., and Hubert, C.R.J. (2017) Using thermodynamics to predict the outcomes of nitrate-based oil reservoir souring control interventions. *Front Microbiol* **8**: 1–9. https://doi.org/10.3389/fmicb.2017.02575.

Dong, L.F., Sobey, M.N., Smith, C.J., Rusmana, I., Phillips, W., Stott, A., *et al*. (2011) Dissimilatory reduction of nitrate to ammonium, not denitrification or anammox, dominates benthic nitrate reduction in tropical estuaries. *Limnol Oceanogr* **56**: 279–291. https://doi.org/10.4319/lo.2011.56.1.0279.

Eldridge, D., and Greene, R. (1994) Microbiotic soil crusts: a review of their roles in soil and ecological processes in the rangelands of Australia. *Aust J Soil Res* **32**: 389. https://doi.org/10.1071/SR9940389.

Eren, A.M., Morrison, H.G., Lescault, P.J., Reveillaud, J., Vineis, J.H., and Sogin, M.L. (2015) Minimum entropy decomposition: unsupervised oligotyping for sensitive partitioning of high-throughput marker gene sequences. *ISME J* **9**: 968–979. https://doi.org/10.1038/ismej.2014.195.

Frankenbach, S., Pais, C., Martinez, M., Laviale, M., Ezequiel, J., and Serôdio, J. (2014) Evidence for gravitactic behaviour in benthic diatoms. *Eur J Phycol* **49**: 429–435. https://doi.org/10.1080/09670262.2014.974218.

Füssel, J., Lam, P., Lavik, G., Jensen, M.M., Holtappels, M., Günter, M., and Kuypers, M.M.M. (2012) Nitrite oxidation in the Namibian oxygen minimum zone. *ISME J* **6**: 1200–1209. https://doi.org/10.1038/ismej.2011.178.

Gause, G.F., Smaragdova, N.P., and Witt, A.A. (1936) Further studies of interaction between predators and prey. *J Anim Ecol* **5**: 1–1. https://doi.org/10.2307/1087.

Gemerden, H. (1993) Microbial mats: A joint venture. *Mar Geol* **113**: 3–25.

Green, B.R. (2011) Chloroplast genomes of photosynthetic eukaryotes. *The Plant Journal* **66**: 34–44. https://doi.org/10.1111/j.1365-313x.2011.04541.x.

Giblin, A., Tobias, C., Song, B., Weston, N., Banta, G., and Rivera-Monroy, V. (2013) The importance of dissimilatory nitrate reduction to ammonium (DNRA) in the nitrogen cycle of coastal ecosystems. *Oceanography* **26**: 124–131. https://doi.org/10.5670/oceanog.2013.54.

Guarini, J.-M., Chauvaud, L., and Coston-Guarini, J. (2008) Can the intertidal benthic microalgal primary production account for the "missing carbon sink"? *J Oceanogr Res Data* **1**: 13–19.

Hay, S.I., Maitland, T.C., and Paterson, D.M. (1993) The speed of diatom migration through natural and artificial substrata. *Diat Res* **8**: 371–384. https://doi.org/10.1080/0269249x.1993.9705268.

Holmes, R.M., Aminot, A., Kérouel, R., Hooker, B.A., and Peterson, B.J. (1999) A simple and precise method for measuring ammonium in marine and freshwater ecosystems. *Can J Fish Aquat Sci* **56**: 1801–1808.

Holtappels, M., Lavik, G., Jensen, M.M., and Kuypers, M.M. (2011) 15N-labeling experiments to dissect the contributions of heterotrophic denitrification and anammox to nitrogen removal in the OMZ waters of the ocean. *Methods Enzymol* **486**: 223–251. https://doi.org/10.1016/b978-0-12-381294-0.00010-9.

Huse, S.M., Dethlefsen, L., Huber, J.A., Welch, D.M., Relman, D.A., and Sogin, M.L. (2008) Exploring microbial diversity and taxonomy using SSU rRNA hypervariable tag sequencing. *PLoS Genet* **4**: e1000255. https://doi.org/10.1371/journal.pgen.1000255.

Kamp, A., de Beer, D., Nitsch, J.L., Lavik, G., and Stief, P. (2011) Diatoms respire nitrate to survive dark and anoxic conditions. *Proc Natl Acad Sci* **108**: 5649–5654. https://doi.org/10.1073/pnas.1015744108.

Kamp, A., Stief, P., Knappe, J., and de Beer, D. (2013) Response of the ubiquitous pelagic diatom *Thalassiosira weissflogii* to darkness and anoxia. *PLoS One* **8**: e82605. https://doi.org/10.1371/journal.pone.0082605.

Kamp, A., Hogslund, S., Risgaard-Petersen, N., and Stief, P. (2015) Nitrate storage and dissimilatory nitrate reduction by eukaryotic microbes. *Front Microbiol* **6**: 1492. https://doi.org/10.3389/fmicb.2015.01492.

Karen, K.G., Lembke, C., Vyverman, W., and Pohnert, G. (2019) Selective chemoattraction of the benthic diatom *Seminavis robusta* to phosphate but not to inorganic nitrogen sources contributes to biofilm structuring. *MicrobiologyOpen* **8**: 1–10. https://doi.org/10.1002/mbo3.694.

King, D., and Nedwell, D.B. (1985) The influence of nitrate concentration upon the end-products of nitrate dissimilation by bacteria in anaerobic salt marsh sediment. *FEMS Microbiol Lett* **31**: 23–28. https://doi.org/10.1016/0378-1097(85)90043-6.

Kingston, M.B. (1999) Wave effects on the vertical migration of two benthic microalgae: *Hantzschia virgata* var. intermedia and *Euglena proxima*. *Estuaries* **22**: 81–91. https://doi.org/10.2307/1352929.

Klatt, J.M., Meyer, S., Häusler, S., Macalady, J.L., de Beer, D., and Polerecky, L. (2016) Structure and function of natural sulphide-oxidizing microbial mats under dynamic input of light and chemical energy. *The ISME Journal* **10**: 921–933. https://doi.org/10.1038/ismej.2015.167.

Klatt, J.M., Gomez-Saez, G.V., Meyer, S., Ristova, P.P., Yilmaz, P., Granitsiotis, M.S., *et al* (2020) Versatile cyanobacteria control the timing and extent of sulfide production in a Proterozoic analog microbial mat. *The ISME Journal* **14**: 3024–3037. https://doi.org/10.1038/s41396-020-0734-z.

Koho, K.A., Piña-Ochoa, E., Geslin, E., and Risgaard-Petersen, N. (2011) Vertical migration, nitrate uptake and denitrification: survival mechanisms of foraminifers (*Globobulimina turgida*) under low oxygen conditions. *FEMS Microbiol Ecol* **75**: 273–283. https://doi.org/10.1111/j.1574-6941.2010.01010.x.

Kozich, J.J., Westcott, S.L., Baxter, N.T., Highlander, S.K., and Schloss, P.D. (2013) Development of a dual-index sequencing strategy and curation pipeline for analyzing amplicon sequence data on the MiSeq Illumina sequencing platform. *Appl Environ Microbiol* **79**: 5112–5120. https://doi.org/10.1128/AEM.01043-13.

Kraft, B., Tegetmeyer, H.E., Sharma, R., Klotz, M.G., Ferdelman, T.G., Hettich, R.L., *et al* (2014) The environmental controls that govern the end product of bacterial nitrate respiration. *Science* **345**: 676–679. https://doi.org/10.1126/science.1254070.

Kuczynska, P., Jemiola-Rzeminska, M., and Strzalka, K. (2015) Photosynthetic pigments in diatoms. *Mar Drugs* **13**: 5847–5881. https://doi.org/10.3390/md13095847.

Kühl, M., and Jørgensen, B.B. (1992) Spectral light measurements in microbenthic phototrophic communities with a fiber-optic microprobe coupled to a sensitive diode array detector. *Limnol Oceanogr* **37**: 1813–1823. https://doi.org/10.4319/lo.1992.37.8.1813.

Kühl, M., Lassen, C., and Jorgensen, B.B. (1994) Light penetration and light intensity in sandy marine sediments measured with irradiance and scalar irradiance fiber-optic microprobes. *Mar Ecol Prog Ser* **105**: 139–148. https://doi.org/10.3354/meps105139.

Kuypers, M.M.M., Marchant, H.K., and Kartal, B. (2018) The microbial nitrogen-cycling network. *Nat Rev Microbiol* **16**: 263–276. https://doi.org/10.1038/nrmicro.2018.9.

Li, Y.H., and Gregory, S. (1974) Diffusion of ions in sea water and in deep-sea sediments. *Geochim Cosmochim Acta* **38**: 703–714.

Longphuirt, S., Lim, J.-H., Leynaert, A., Claquin, P., Choy, E.-J., Kang, C.-K., and An, S. (2009) Dissolved inorganic nitrogen uptake by intertidal microphytobenthos: nutrient concentrations, light availability and migration. *Mar Ecol Prog Ser* **379**: 33–34. https://doi.org/10.3354/meps07852.

Macintyre, H., Geider, R., and Miller, D. (1996) Microphytobenthos: the ecological role of the "secret garden" of

Unvegetated, shallow-water marine habitats. I. Distribution, abundance and primary production. *Estuaries Coasts* **19**: 186–201. https://doi.org/10.2307/1352224.

Marchant, H.K., Holtappels, M., Lavik, G., Ahmerkamp, S., Winter, C., and Kuypers, M.M.M. (2016) Coupled nitrification–denitrification leads to extensive N loss in subtidal permeable sediments. *Limnol Oceanogr* **61**: 1033–1048. https://doi.org/10.1002/lno.10271.

McTigue, N.D., Gardner, W.S., Dunton, K.H., and Hardison, A.K. (2016) Biotic and abiotic controls on co-occurring nitrogen cycling processes in shallow Arctic shelf sediments. *Nat Commun* **7**: 1–11. https://doi.org/10.1038/ncomms13145.

Murphy, A.E., Bulseco, A.N., Ackerman, R., Vineis, J.H., and Bowen, J.L. (2020) Sulphide addition favours respiratory ammonification (DNRA) over complete denitrification and alters the active microbial community in salt marsh sediments. *Environ Microbiol* **00**: 2124–2139. https://doi.org/10.1111/1462-2920.14969.

Mussmann, M., Hu, F.Z., Richter, M., de Beer, D., Preisler, A., Jorgensen, B.B., *et al*. (2007) Insights into the genome of large sulfur bacteria revealed by analysis of single filaments. *PLoS Biol* **5**: e230. https://doi.org/10.1371/journal.pbio.0050230.

Nold, S.C., Bellecourt, M.J., Kendall, S.T., Ruberg, S.A., Sanders, T.G., Klump, J.V., and Biddanda, B.A. (2013) Underwater sinkhole sediments sequester Lake Huron's carbon. *Biogeochemistry* **115**: 235–250. https://doi.org/10.1007/s10533-013-9830-8.

Palmer, J.D., and Round, F.E. (1967) Persistent, vertical-migration rhythms in benthic microflora. Vi. The tidal and diurnal nature of the rhythm in the diatom *Hantzschia virgata*. *Biol Bull* **132**: 44–55. https://doi.org/10.2307/1539877.

Pinckney, J., and Zingmark, R.G. (1991) Effects of tidal stage and sun angles on intertidal benthic microalgal productivity. *Mar Ecol Prog Ser* **76**: 81–89. https://doi.org/10.3354/meps076081.

Preisler, A., De Beer, D., Lichtschlag, A., Lavik, G., Boetius, A., and Joørgensen, B.B. (2007) Biological and chemical sulfide oxidation in a Beggiatoa inhabited marine sediment. *ISME J* **1**: 341–353. https://doi.org/10.1038/ismej.2007.50.

Prokopenko, M.G., Sigman, D.M., Berelson, W.M., Hammond, D.E., Barnett, B., Chong, L., and Townsend-Small, A. (2011) Denitrification in anoxic sediments supported by biological nitrate transport. *Geochim Cosmochim Acta* **75**: 7180–7199. https://doi.org/10.1016/j.gca.2011.09.023.

Pruesse, E., Quast, C., Knittel, K., Fuchs, B.M., Ludwig, W., Peplies, J., and Glöckner, F.O. (2007) SILVA: a comprehensive online resource for quality checked and aligned ribosomal RNA sequence data compatible with ARB. *Nucleic Acids Res* **35**: 7188–7196. https://doi.org/10.1093/nar/gkm864.

R Core Team. (2015) *R: A Language and Environment for Statistical Computing*. Vienna, Austria. URL https://www.r-project.org

Revsbech, N.P. (1989) An oxygen microsensor with a guard cathode. *Limnol Oceanogr* **34**: 474–478. https://doi.org/10.4319/lo.1989.34.2.0474.

Risgaard-Petersen, N. (2003) Coupled nitrification–denitrification in autotrophic and heterotrophic estuarine sediments: on the influence of benthic microalgae. *Limnol Oceanogr* **48**: 93–105. https://doi.org/10.4319/lo.2003.48.1.0093.

Round, F.E., and Palmer, J.D. (1966) Persistent, vertical-migration rhythms in benthic microflora: II. Field and laboratory studies on diatoms from the banks of the river Avon. *J Mar Biol Assoc U K* **46**: 191–214. https://doi.org/10.1017/S0025315400017641.

Ruberg, S.A., Coleman, D.F., Johengen, T.H., Meadows, G. A., Van Sumeren, H.W., Lang, G.A., and Biddanda, B.A. (2005) Groundwater plume mapping in a submerged sinkhole in Lake Huron. *Mar Technol Soc J* **39**: 65–69.

Saburova, M.A., and Polikarpov, I.G. (2003) Diatom activity within soft sediments: behavioural and physiological processes. *Mar Ecol Prog Ser* **251**: 115–126. https://doi.org/10.3354/meps251115.

Schloss, P.D., Westcott, S.L., Ryabin, T., Hall, J.R., Hartmann, M., Hollister, E.B., *et al*. (2009) Introducing mothur: open-source, platform-independent, community-supported software for describing and comparing microbial communities. *Appl Environ Microbiol* **75**: 7537–7541. https://doi.org/10.1128/AEM.01541-09.

Schutte, C.A., Teske, A., MacGregor, B.J., Salman-Carvalho, V., Lavik, G., Hach, P., and de Beer, D. (2018) Filamentous giant Beggiatoaceae from the Guaymas Basin are capable of both denitrification and dissimilatory nitrate reduction to ammonium. *Appl Environ Microbiol* **84**: 1–13. https://doi.org/10.1128/AEM.02860-17.

Seekatz, A.M., Theriot, C.M., Molloy, C.T., Wozniak, K.L., Bergin, I.L., and Young, V.B. (2015) Fecal microbiota transplantation eliminates *Clostridium difficile* in a murine model of relapsing disease. *Infect Immun* **83**: 3838–3846. https://doi.org/10.1128/IAI.00459-15.

Serôdio, J., and Catarino, F. (2000) Modelling the primary productivity of intertidal microphytobenthos: time scales of variability and effects of migratory rhythms. *Mar Ecol Prog Ser* **192**: 13–30. https://doi.org/10.3354/meps192013.

Sharrar, A.M., Flood, B.E., Bailey, J.V., Jones, D.S., Biddanda, B.A., Ruberg, S.A., *et al*. (2017) Novel large sulfur bacteria in the metagenomes of groundwater-fed chemosynthetic microbial mats in the Lake Huron basin. *Front Microbiol* **8**: 1–15. https://doi.org/10.3389/fmicb.2017.00791.

Stal, L.J., and Caumette, P. (eds). (2013) *Microbial Mats (Structure, Development and Environmental Significance). Series G: Ecological Sciences*, Berlin, Germany: Springer Science & Business Media. https://doi.org/10.1007/978-3-642-78991-5.

Stal, L.J., and Moezelaar, R. (1997) Fermentation in cyanobacteria. *FEMS Microbiol Rev* **21**: 179–211. https://doi.org/10.1016/S0168-6445(97)00056-9.

Stal, L.J., van Gemerden, H., and Krumbein, W.E. (1985) Structure and development of a benthic marine microbial mat. *FEMS Microbiol Lett* **31**: 111–125. https://doi.org/10.1016/0378-1097(85)90007-2.

Stief, P., Kamp, A., and de Beer, D. (2013) Role of diatoms in the spatial-temporal distribution of intracellular nitrate in intertidal sediment. *PLoS One* **8**: 1–15. https://doi.org/10.1371/journal.pone.0073257.

Stief, P., Fuchs-Ocklenburg, S., Kamp, A., Manohar, C.S., Houbraken, J., Boekhout, T., *et al*. (2014) Dissimilatory nitrate reduction by *Aspergillus terreus* isolated from the seasonal oxygen minimum zone in the Arabian Sea. *BMC Microbiol* **14**: 1–10. https://doi.org/10.1186/1471-2180-14-35.

Stomp, M., Huisman, J., Stal, L.J., and Matthijs, H.C. (2007) Colorful niches of phototrophic microorganisms shaped by vibrations of the water molecule. *ISME J* **1**: 271–282. https://doi.org/10.1038/ismej.2007.59.

Sundbäck, K., Miles, A., and Göransson, E. (2000) Nitrogen fluxes, denitrification and the role of microphytobenthos in microtidal shallow-water sediments:an annual study. *Mar Ecol Prog Ser* **200**: 59–76. https://doi.org/10.3354/meps200059.

Tiedje, J. (1988) *Ecology of Denitrification and Dissimilatory Nitrate Reduction to Ammonium*, Chapter 4. New York, NY: John Wiley & Sons.

Voorhies, A.A., Biddanda, B.A., Kendall, S.T., Jain, S., Marcus, D.N., Nold, S.C., *et al*. (2012) Cyanobacterial life at low O_2: community genomics and function reveal metabolic versatility and extremely low diversity in a Great Lakes sinkhole mat. *Geobiology* **10**: 250–267. https://doi.org/10.1111/j.1472-4669.2012.00322.x.

Warembourg, F.R. (1993) *Nitrogen Fixation in Soil and Plant Systems*, Cambridge, MA: Academic Press. https://doi.org/10.1016/b978-0-08-092407-6.50010-9.

Wenzhöfer, F., Holby, O., Glud, R.N., Nielsen, H.K., and Gundersen, J.K. (2000) *In situ* microsensor studies of a shallow water hydrothermal vent at Milos, Greece. *Mar Chem* **69**: 43–54.

Xie, H. (2008) Activity assay of membrane transport proteins. *Acta Biochimica et Biophysica Sinica* **40**: 269–277. http://dx.doi.org/10.1111/j.1745-7270.2008.00400.x.

Supporting Information

Additional Supporting Information may be found in the online version of this article at the publisher's web-site:

Appendix S1: Supporting Information